SAE INTERNATIONAL®

# Comparison of High- and Low-Pressure Electric Supercharging of a HDD Engine: Steady State and Dynamic Air-Path Considerations

2016-01-1035

Published 04/05/2016

**Rasoul Salehi, Jason Martz, and Anna Stefanopoulou**
University of Michigan

**Taylor Hansen and Andrew Haughton**
Controlled Power Technologies, Inc

**CITATION:** Salehi, R., Martz, J., Stefanopoulou, A., Hansen, T. et al., "Comparison of High- and Low-Pressure Electric Supercharging of a HDD Engine: Steady State and Dynamic Air-Path Considerations," SAE Technical Paper 2016-01-1035, 2016, doi:10.4271/2016-01-1035.



## Abstract

This paper numerically investigates the performance implications of the use of an electric supercharger in a heavy-duty DD13 diesel engine. Two electric supercharger configurations are examined. The first is a high-pressure (HP) configuration where the supercharger is placed after the turbocharger compressor, while the second is a low-pressure (LP) one, where the supercharger is placed before the turbocharger compressor. At steady state, high engine speed operation, the airflows of the HP and LP implementations can vary by as much as 20%. For transient operation under the Federal Test Procedure (FTP) heavy duty diesel (HDD) engine transient drive cycle, supercharging is required only at very low engine speeds to improve airflow and torque. Under the low speed transient conditions, both the LP and HP configurations show similar increases in torque response so that there are 44 fewer engine cycles at the smoke-limit relative to the baseline turbocharged engine. When the requested engine torque rise rate is increased from the FTP ramps to steps, the benefit of supercharging is extended to also include mid-range engine speeds, with over ~ 70% fewer cycles at the smoke-limit line. In addition, the results show an improvement in the overall fuel economy of the supercharged engine during low engine speed transients compared to the baseline turbocharged engine. The study highlights the importance of supercharger by-pass valve control, where the transient response of the valve should be twice as fast as the electric supercharger drive motor for accurate and minimal supercharger power consumption during transient maneuvers. Finally, an engine re-calibration with increased exhaust gas recirculation at low engine speeds/loads, resulted 4.6% fuel economy improvements at that low speed/load region while the supercharger enabled fast air-flow increase during aggressive tip-ins.

## Introduction

Diesel engine downsizing and downspeeding strategies have been used to improve vehicular fuel economy [1, 2]. These strategies are most effectively realized through the use of forced air-charging systems such as turbochargers, which increase the engine torque. However the resulting turbo-lag of these devices can be problematic during engine transients [3]. Two-stage charging via the integration of a supercharger into a turbocharged diesel engine allows fast air-charge increases and minimizes turbo-lag during a torque request [4]. Both electrically and mechanically driven superchargers are available in the marketplace. Electric units, which are more flexible in terms of controllability, are under development with both roots-type (or positive displacement) [5] and centrifugal compressors [4, 6, 7].

In a two-stage charged engine there are two possible supercharger implementations; a low pressure (LP) configuration where the supercharger is placed upstream of the main compressor and a high-pressure (HP) one where the supercharger is inserted downstream the main compressor (Figure 1). The selection of either HP or LP implementation is driven by several factors. For example, the lower corrected mass flow rate of HP supercharging covers the full engine speed-load map without choking [8, 9]. In addition, for a similar pressure ratio and at high air mass flow rates, the rotational speed of the HP supercharger is lower than an LP one, affecting both electric motor (EM) and compressor efficiency [10]. The LP integration however faces fewer material stress and sealing challenges, given the lower working pressure of these units. These trade-offs complicate the selection of either LP or HP supercharging for a turbocharged diesel engine.

The current work evaluates the steady state and transient performance of HP and LP electric supercharging (eSC) configurations with a model previously developed for a turbocharged DD13 engine [11]. The LP and HP configurations are compared by simulating the steady state operation of the supercharged engine over the entire engine speed-load map. Then, the effect of engine dynamics and transient conditions on the HP and LP comparison is evaluated by simulating the supercharged engine during transient operations to reduce smoke emissions and improve torque response. Two different load transient commands are selected for supercharger evaluation, including a series of worst case torque commands from the FTP heavy duty transient cycle and also torque step commands, which are the fastest commands that a driver may request, especially at low engine speeds. The implication of the supercharger bypass valve response time to supercharger transient response and parasitic losses is also examined. A final study investigates how both engine fuel economy and torque response can be improved by the electric supercharger during transient, allowing the use of exhaust gas recirculation (EGR) with an open wastegate (WG) at steady state operations.

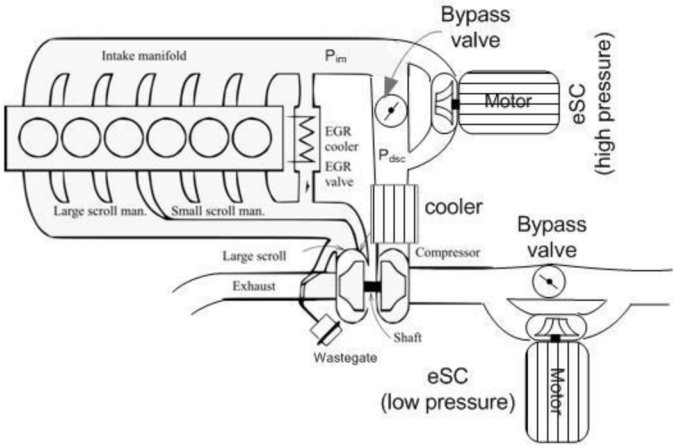


Figure 1. LP and HP eSC integrations in the DD13 engine.

## Electrically Supercharged HDD Engine Model

A model of the 12.8 L heavy duty diesel (HDD) DD13 engine [11] is used in the current work for studying the effect of eSC integration location. The DD13 engine is equipped with a high pressure loop EGR system. The system includes an electrically actuated EGR valve which diverts gas from the exhaust manifold into the intake manifold after the intercooler. This cooled EGR leads to lower peak in-cylinder temperatures that reduce nitrogen oxide emissions and heat loss to the cylinder walls. The engine is equipped with an asymmetric twin-scroll turbine, where the exhaust manifold is constructed so that the flow from three of the cylinders feeds into a small turbine scroll while the flow from the other three cylinders feeds into a larger scroll. The higher pressure in the more restrictive small scroll manifold drives high-pressure EGR through an EGR cooler into the intake manifold. The pressure in the large scroll is lower than the small scroll, allowing three of the cylinders to operate with reduced pumping work. The net effect is typically reduced overall pumping loss with a corresponding improvement in fuel economy. The engine is also equipped with a pneumatic WG valve, which bypasses the large scroll to avoid over-boosting and to reduce pumping losses.

The baseline engine model (shown schematically in Figure 2) is formed by connecting individual component models. Component models include the engine cylinder, turbocharger, intercooler, WG and EGR valves, along with dynamical models for the intake manifold pressure ($P_{im}$), large and small scroll exhaust manifold pressures ($P_{eml}$ and $P_{ems}$), exhaust manifold pressure downstream the turbine ($P_{dst}$), air fractions in the intake and exhaust manifold ($F_{im}$, $F_{em}$) and the turbocharger speed ($N_{tc}$). Additional details are presented in reference [11]. Figure 3 shows the model's ability to predict the measured data (including the air fuel equivalence ratio (λ), the engine torque ($T_e$) and the compressor mass flow) at different engine speeds ($N_e$) with ±5% accuracy. The modular form of the model allows the addition of new component sub-models (here the electric supercharger sub-model) to the baseline engine model.

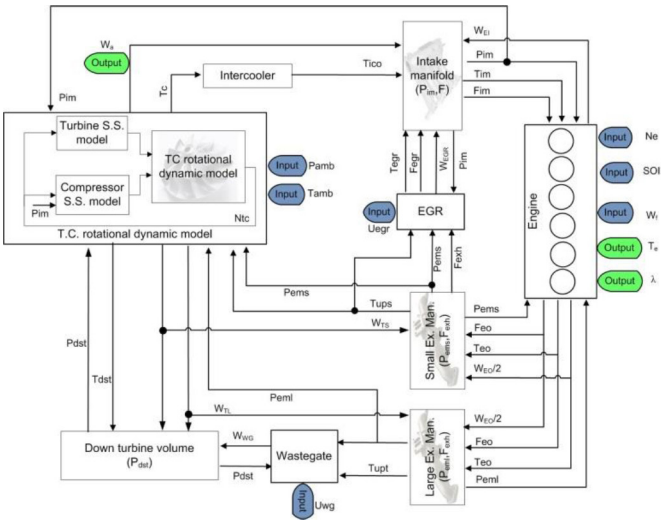


Figure 2. DD13 engine model structure.

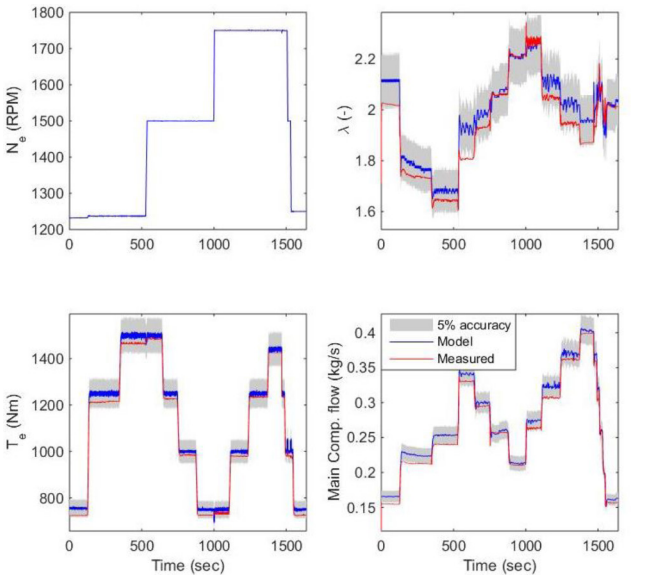


Figure 3. Validation results for the DD13 baseline engine model.

A water cooled eSC from Controlled Power Technologies (CPT) [7] is integrated into the engine model for evaluation of the LP and HP eSC configurations (Figure 1). The COBRA (COntrolled Boosting for Rapid response Applications) model C80 electric supercharger is comprised of a radial and a liquid cooled switched reluctance electric motor. An electric bypass valve is also included in the model to bypass air around the eSC unit when this unit is off line.

The eSC compressor characteristic map is shown in Figure 4 with the normalized corrected flow, defined as:

$$Norm.\ Corr.flow = \frac{Compressor\ Corr.\ flow}{Max.\ eSC\ \ Corr.\ flow}. \quad (1)$$

As an important feature shown in Figure 4, the eSC's compressor has high efficiency at low pressure ratios. This is apparent when the high-efficiency region for the eSC is compared to that of the main compressor as plotted in Figure 5 where all flow rates normalized by the maximum eSC corrected flow rate used in the normalization of Figure 4. As shown, the eSC compressor has high efficiency at very low pressure ratios. Moreover, the electrical motor is designed for high electrical efficiency at the high shaft speeds where eSC's typically work.

Simple rule-based controllers are included in the model to coordinate the electric supercharger drive motor, the supercharger bypass valve along with the EGR and WG actuators. The controller speeds up the eSC and closes the EGR, WG and bypass valves when the engine performs a transient. In addition, a fuel limiter is included to limit the injected fuel mass to maintain λ above the smoke limit (as $\lambda_{crit}$), which is chosen as $\lambda_{crit} = 1.6$ [12].

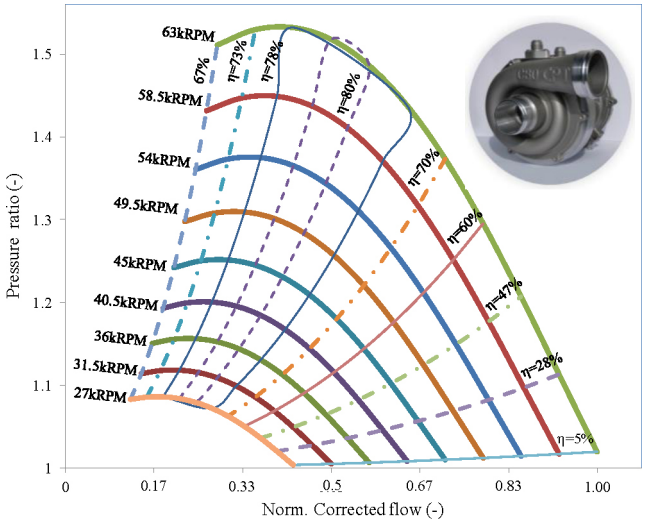


Figure 4. COBRA C80 compressor map.

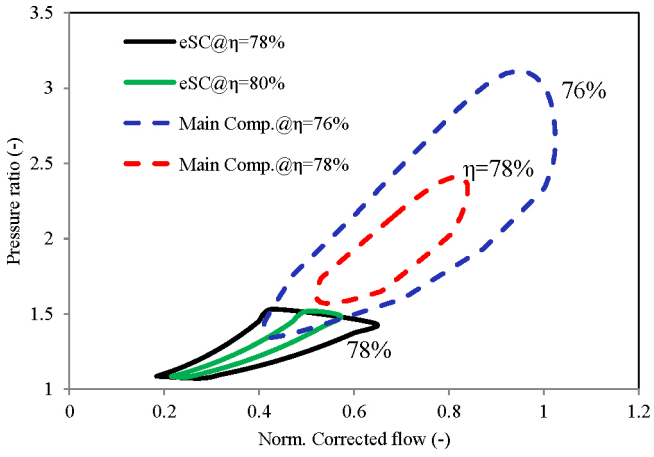


Figure 5. Comparison of high-efficiency regions for the eSC and main compressor.

## LP-HP Comparison at Steady State

Conventionally, the ability of LP and HP eSC implementations to increase the engine air charge is compared under steady state conditions. The HP configuration generally has lower corrected flows. Therefore the HP unit, with a smaller compressor, can cover the entire engine map [9], unlike the LP unit. This is shown in Figure 6 by plotting the maximum air flow increase into the engine using the LP eSC (Figure 6-a) relative to the baseline turbocharged engine and the difference between the engine air flow in the HP and LP eSC configurations (Figure 6-b) calculated as:

$$\Delta W_{air} = \frac{W_{air,HP} - W_{air,LP}}{W_{air,LP}} * 100. \quad (2)$$

In equation (2), both $W_{air,HP}$ and $W_{air,LP}$ are calculated with the eSC at maximum power and with an injected fuel mass similar to the baseline engine. As the contour plot shows, in the lower left half of the map, the LP and HP air flow are quite similar. But as the engine speed and load increase, the HP unit passes much more air flow. Three operating points "A", "B" and "C" are highlighted in Figure 6 with LP and HP difference as -1%, 14% and 16% respectively. These three points will be used for further discussions in later sections.

Another advantage of supercharging is increasing the low-end torque required for downspeeding [8]. The baseline turbocharger cannot provide sufficient air flow at low engine speeds, limiting the maximum engine torque delivered during a tip-in. At high engine speeds (as shown in Figure 7-a) both the EGR valve and WG are open and can be used to increase the engine air-charge and torque, therefore supplementary boosting devices are not necessary. Moreover, large torque jumps during high load transients happen primarily at low engine speeds (as will be discussed in the next section). To show how the eSC increases the air-charge at full loads, the HP and LP eSC implementations are simulated at low engine speeds, as shown in Figure 7-a. With the eSC integrated, the higher boost pressures enable increased low-end torque while avoiding application of the fuel limiter for the avoidance of minimum lambda / high soot generation limits and the main compressor surge line.

Figure 7-b shows the difference between the LP and HP configurations on the eSC's compressor map. The results indicate that the corrected mass flow is much lower and almost constant for the HP integration because its inlet is connected into the main compressor outlet, and therefore has higher inlet pressure compared to the LP unit. The plot shows that at 608 RPM, the LP implementation operates in a central region of the map with efficiency higher than the HP unit. But with an increase of engine speed and air flow, the operating point quickly moves to the right of the compressor map where the efficiency is very low. A problem observed for the HP implementation at low engine speeds is that it approaches the surge line. This can be avoided if the compressor is sized so the HP operating points are shifted to the right of the map, at the expense of reduced compressor efficiency.

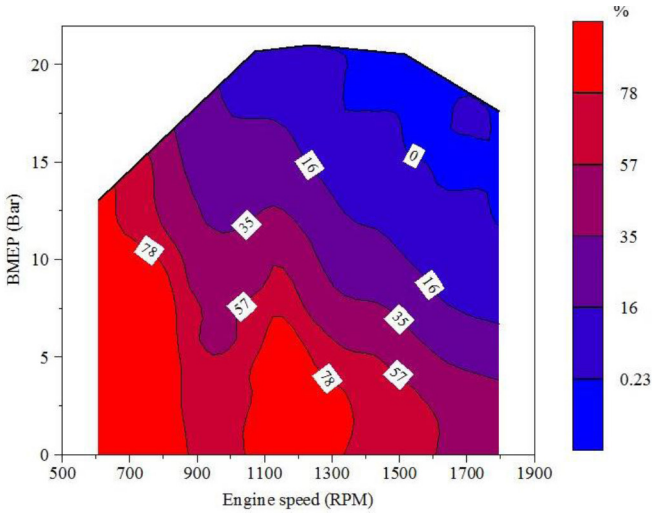


(a).

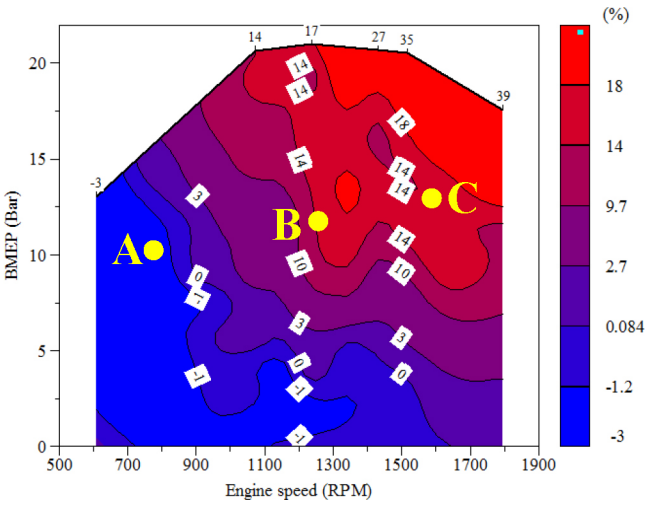


(b).

Figure 6. Percent increase in the engine air-charge flow (a) for the LP eSC relative to the baseline engine and (b) for the HP eSC relative to the LP eSC when the maximum possible power is applied to the eSC electric motor.

## Transient Comparison of LP-HP Implementations

One of the main advantages of electric supercharging during speed and load transients is the associated fast response of the air-charge. Transient performance and emissions are often assessed for heavy-duty (HD) engines with cycles such as the FTP [13]. The engine torque and speed are plotted over the HD FTP cycle in Figure 8. For such a transient cycle, the torque change from one engine cycle to the next ($\Delta T_{cycl}$) is calculated as:

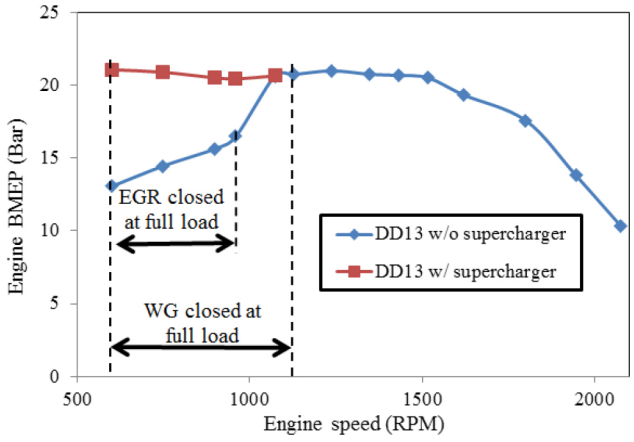


(a).

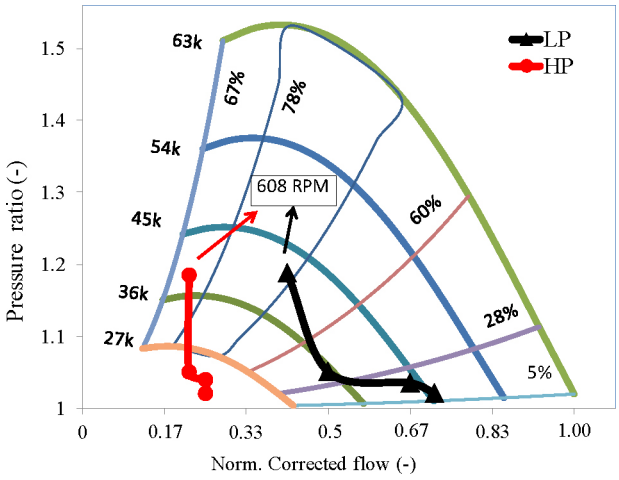


(b).

Figure 7. (a) Improving maximum low-end torque by using either the HP or LP eSC. (b) Difference between the eSC's compressor operation for the LP and HP integrations.

$$\Delta T_{cycl} = [T_e(t+\Delta t) - T_e(t)] / \left\lfloor \frac{N_e}{120} * \Delta t \right\rfloor. \quad (3)$$

Where $T_e(t)$ is the engine torque at time "$t$" and $Ne$ is the average of engine speed over $[t,t+\Delta t]$ seconds. Positive values of $\Delta T_{cycl}$ are shown for the DD13 engine during the FTP heavy duty transient cycle in the color map of Figure 9 as a function of engine speed and load. The figure shows that the highest cycle-based torque changes occur at low engine speeds, in the range of 600-800 RPM, where turbo-lag is an issue and the rate of air-charge increase is slow. This low speed region, 750 RPM, 1065 Nm, 35 Nm/cycl, is selected as the maximum torque rise operating condition that may be requested at low engine speed during the FTP. The plot also indicates that at medium engine speeds, the maximum engine torque increases but the torque change rate is more moderate, hence 1237 RPM, 1200Nm and 25Nm/cycl are selected as the representative transient conditions. At high engine speeds, between 1400-1800 RPM, torque changes as high as 30 Nm/cycle are observed but occur at part loads.

Smoke, one of the problematic HDD transient emissions, results mainly from a lack of air within the cylinder during transient load increases. Since air fuel ratios (AFR) can approach the smoke limit ($\lambda$=*1.6*) at steady state full load, rich excursions and smoke emissions are especially problematic during fast transitions to high load when the air-charge response is slow. The rich excursions are prevented in modern engines by fuel limiters based on an air-charge estimation. The fuel limiter, however, lengthens the air transient and increases the apparent turbo-lag. Three scenarios are highlighted with arrows in Figure 9 with the challenging transition conditions described in the previous paragraph. These conditions can potentially trigger the fuel limiter and may also benefit from an electric supercharger. For each of these transients, it is assumed that the engine starts from a low load point (Torque ≈ 50 Nm) and ends up at the highlighted torque by following the associated torque rise per cycle. The assumption here is that due to the vehicle inertia, the torque of the engine geared to the wheels increases at a constant speed and is expected to be the worst case torque rise scenario of the FTP cycle certification process. In addition, as will be shown later in Figure 10, the steady state $\lambda$ at the final torque approaches the smoke limit during all of the scenarios.

With the eSC integrated into the DD13 engine model, results from two simulation sets are presented, the FTP worst case scenarios and even more challenging (step) transients applied at the three engine speeds. These simulations are compared against the baseline turbocharger only case, which does not have electric supercharging.

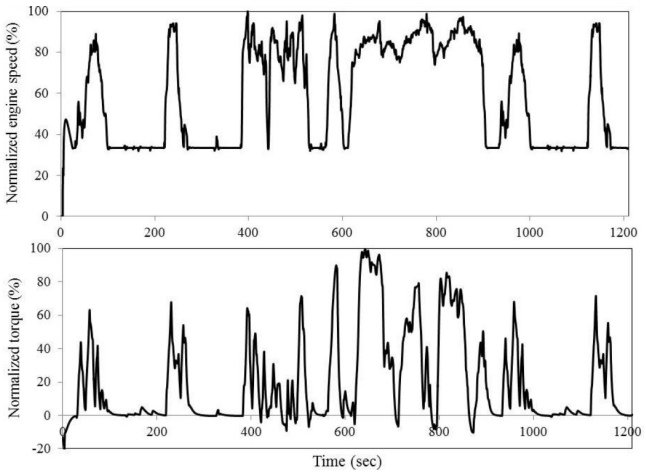


Figure 8. Engine trajectory during the FTP heavy duty transient drive cycle.

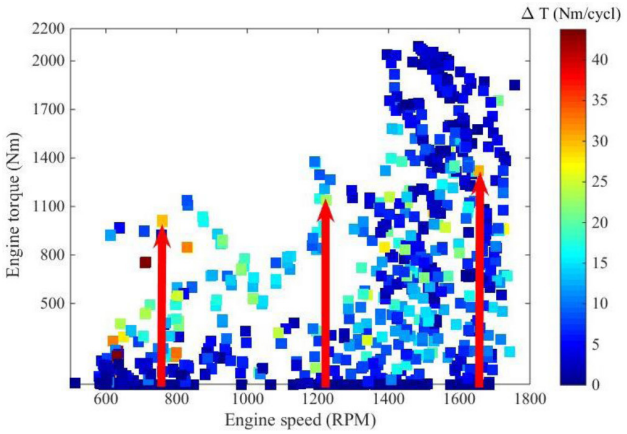


Figure 9. Cycle-based torque change of the DD13 over the FTP heavy-duty transient cycle (only positive values are shown). Arrows indicate the maximum possible cyclic brake torque changes within a given speed range.

## *FTP Fastest Load Transients*

The worst case load transient scenarios identified from Figure 9 are now applied to the DD13 engine model. Three different tests were simulated, 1) the baseline engine with the main turbocharger, without electric supercharger, 2) the baseline engine with a HP eSC implementation and 3) the baseline engine with a LP eSC implementation. For all tests, the WG and EGR valves are closed during the transients to allow fast turbocharger response. For simulations 2 and 3, the electric power into the electric supercharger is similar with a profile designed to minimize the $\lambda$ overshoot. The results show that at 750 RPM in Figure 10-a, the baseline engine violates the smoke limit ($\lambda_{min}$=1.6) and the fuel limiter activates (i.e. *fuel limiter=1* in Figure 10-a), decreasing fueling rate for approximately 7 seconds, which corresponds to 44 engine cycles. The limited fuel delivery creates a long delay in brake torque ($T_e$) response at high load, which is clearly shown in Figure 10-a. While all three configurations approach $\lambda_{min}$=1.6 when the engine speed increases to 1237 RPM and 1600 RPM in Figure 10-b and c, the simulations never violate the smoke limit. The air charge dynamics are sufficiently fast with the turbocharger alone to maintain $\lambda$ above the limit value at mid and high engine speeds, therefore electric supercharging is not required for these transients. Also apparent in Figure 10-b and c is the leaner λ for the HP integration compared to the LP one during the transients. Because the same input power is applied to the electric motor in both cases, this means that the eSC is working slightly more efficiently for the HP integration at these engine speeds due to its lower corrected flow. At the highest speed in Figure 10-c, there is no noticeable difference between the LP and baseline simulations, indicating that the LP system has a very small effect on air mass flows at high engine speeds and loads.

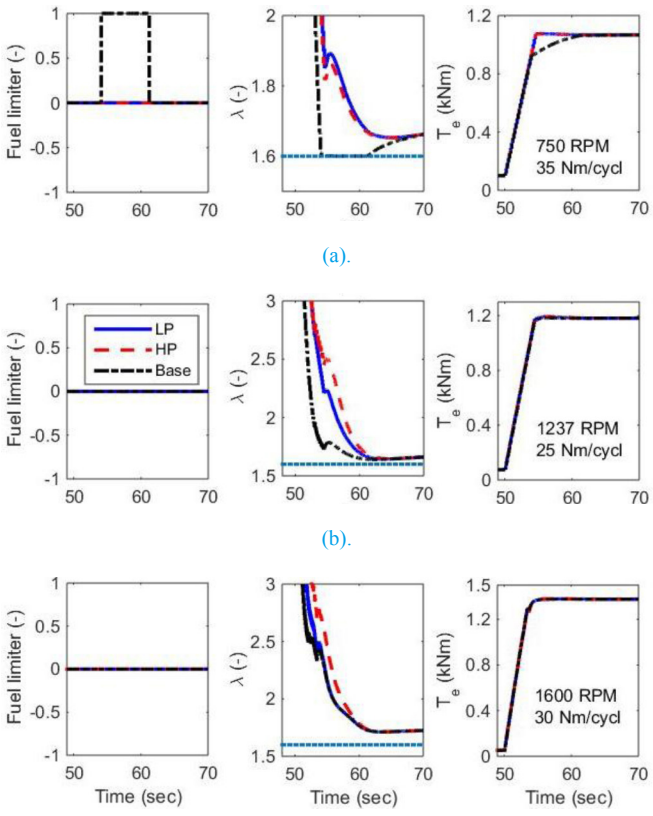


Figure 10. Engine response to the FTP worst case torque demand scenarios.

### *Load Step Transients*

A more challenging torque demand scenario is now simulated by applying a torque step request to the baseline, LP and HP configurations. The same bypass valve and electric motor control strategy is used for both LP and HP systems. As the results in Figure 11 show, the eSC improves the engine response noticeably at engine speeds of 750 and 1237 RPM, however less improvement is observed at 1600 RPM. As plotted at 750 RPM the fuel limiter of the baseline engine is active for 56 cycles but is effectively reduced to 6 cycles with supercharger activation. At 1237 RPM, the supercharger reduces the fuel-limiter active duration from 21 to 7 cycles for the step. When the engine speed increases to 1600 RPM, the fuel-limiter active duration reduces from 12 to 8 and 9 for HP and LP respectively, as Figure 11-c shows. This indicates a much lower effect of the supercharger at 1600 RPM compared to the lower engine speeds.

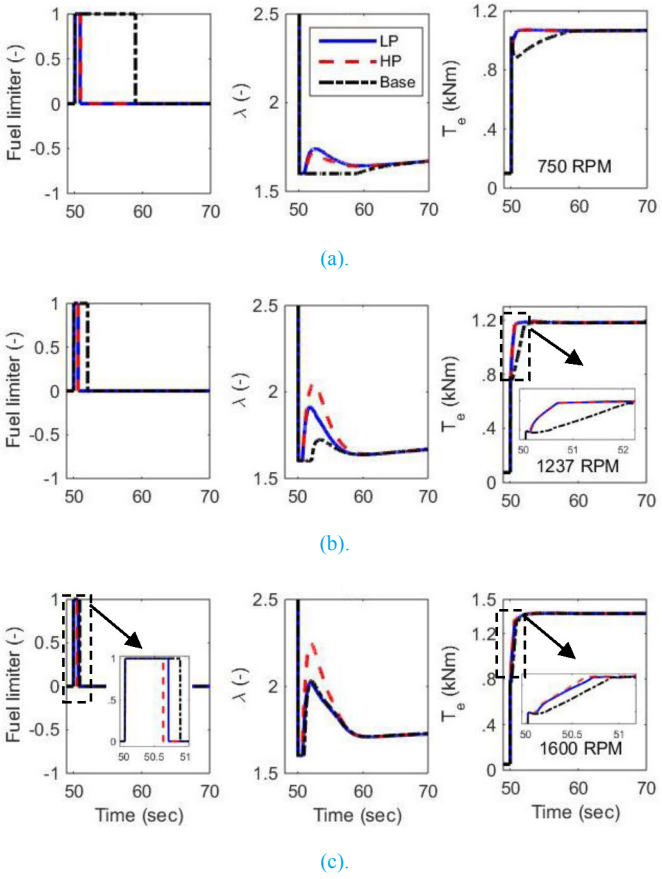


Figure 11. Effect of the eSC on the engine performance during a step torque command.

Reducing the number of fuel-limited cycles during a transient is the main advantage of air-charge increase associated with supercharging. Comparing the HP and LP implementations from Figure 11-c to Figure 6 points out the fact that the HP and LP air mass flow differences during steady state high speed/load operation may be less apparent from fuel-limited cycle reductions during fast transients, where engine and eSC dynamics are included. This can be observed by comparing the HP and LP differences from Figure 6 at point "C" (≈16%) to the effect of air flow increases on reducing the fuel limited cycles in Figure 11-c. The transient plot at 1600 RPM shows that for a transient to the same load as point "C" with maximum electric power applied, the HP and LP configurations have 33% and 25% fewer active fuel limiter cycles, respectively, relative to the baseline turbocharged engine.

The total efficiency of the supercharged engine is explored here by defining the net brake specific fuel consumption ($BSFC_{net}$), which includes the parasitic losses of the supercharger as:

$$BSFC_{net} = \frac{W_f}{PW_{Eng} - PW_{EM}/\eta_{alt}}. \quad (4)$$

Where $W_f$ is the mass flow rate of the fuel injected into the cylinders, $PW_{Eng}$ is the power generated by the engine, $PW_{EM}$ is the power used by the supercharger's electric motor and $\eta_{alt}$ is the alternator efficiency, assumed as a constant 70%. In Figure 12 $BSFC_{net}$ and the engine BSFC ($BSFC_{Eng} = W_f/PW_{Eng}$) for both LP and HP configurations are compared to the $BSFC_{Eng}$ of the baseline engine for the torque steps of Figure 11. As shown, in all engine speeds the supercharged engine has a lower $BSFC_{Eng}$ during the load transient with the 750 RPM engine speed showing the highest improvement in $BSFC_{Eng}$. The reason for the improved $BSFC_{Eng}$ is that at constant engine speeds, $BSFC_{Eng}$ decreases as the engine torque increases. Since the supercharged engine has a faster transient response, then it transitions to low BSFC more quickly than the baseline engine during tip in.

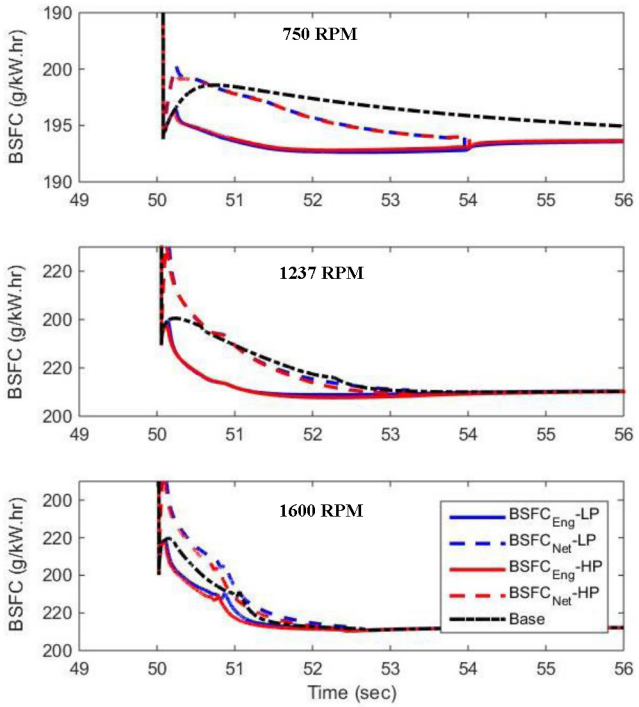


Figure 12. Effect of the eSC on DD13 net BSFC.

Although the power consumed by the electric motor reduces the $BSFC_{Eng}$ improvement, as the difference between $BSFC_{Eng}$ and $BSFC_{net}$ in Figure 12 shows, the $BSFC_{Eng}$ improvement is sufficiently high to cancel the supercharger parasitics. The final efficiency of the engine (i.e. $BSFC_{net}$ ) therefore does not decrease at the engine speeds where the transient response is improved (at speeds of 750 and 1237 RPM). For the simulation results shown in Figure 12, the fuel limiter applied to the baseline engine prevents it from quickly arriving at the high-load, low-BSFC operating points. If the fuel limiter were not used on the baseline engine, this engine would have a faster response however soot generation would increase. This brings the consequent penalties of increased pressure drop over the diesel particulate filter (DPF), and low efficiency operation associated with DPF regeneration.

## HP-LP Comparison: The Importance of the Supercharger Bypass Valve Response Time

The electric supercharger bypass valve is a critical element allowing the supercharger to improve the transient response of the engine. This valve should be kept open when the supercharger is offline for low motor parasitic losses. When a transient happens, the valve should close to avoid engine choking and back flow across the supercharger. The ideal case is an instantaneous closure of the valve when the pressure upstream of the supercharger's compressor exceeds its inlet pressure, which is impossible due to the valve dynamics.

A parametric study of the bypass valve dynamics is performed to assess the sensitivity of engine performance to this valve's transient response. The study is performed by setting the time constant of the valve dynamics (simulated as a first order delay) as 10, 60, 130 and 260 ms. $\tau$ =60 ms represents the time constant of electric valves currently available in the marketplace, while $\tau$ =130 ms is the same as the ESC's electric motor time constant. The following hysteresis control strategy is used for the bypass valve:

$$\theta_{valve} = \begin{cases} 0 & \Delta P_{eSC} > \Delta^{+}_{Thr} \\ No\ change & \Delta^{-}_{Thr} < \Delta P_{eSC} < \Delta^{+}_{Thr} \\ 100 & \Delta P_{eSC} < \Delta^{-}_{Thr} \end{cases} \quad (5)$$

where the desired valve position ($\theta_{valve}$) is calculated based on the difference between the upstream and downstream pressures of the eSC ($\Delta P_{eSC}$) and upper and lower thresholds of the pressure difference ($\Delta^{+}_{Thr}$, $\Delta^{-}_{Thr}$). Results of the parametric study are shown in Figure 13 for major variables including the reverse flow through the bypass valve, λ, the electric power used by eSC and the engine torque. In all simulations, the torque demand is applied as a step change with similar final values. As the results show, when the valve delay increases, the reverse flow increases which causes more delay in the torque rise and also more power consumption in the electric motor. The results suggest that a valve with $\tau$ =60 ms (which is twice as fast as the electric motor) performs in a manner very similar to the ideal fast valve with $\tau$ =10 ms. A valve with $\tau$ =60 ms is commercially available and is suggested for use in parallel with the eSC's compressor.

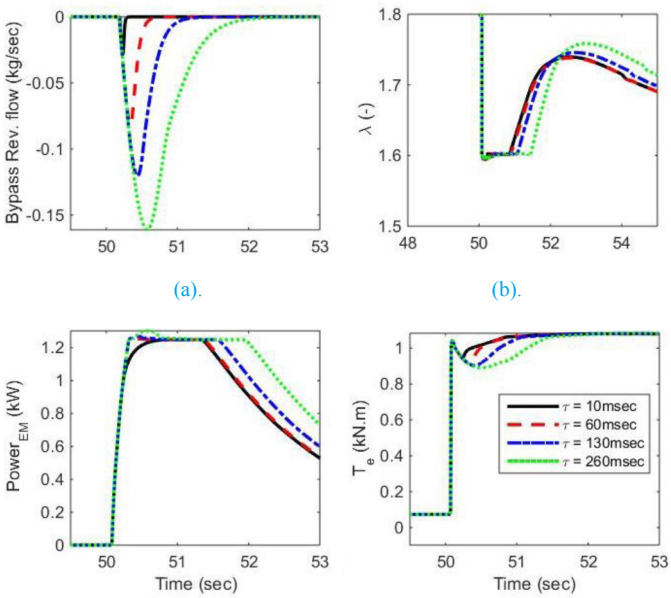


Figure 13. Effect of the speed of the bypass valve on the LP supercharged engine performance at 750 RPM.

## Using the Supercharger for Fuel Savings at Steady State

As Figure 7-a showed, low speed operation involves closed EGR valve and WG. Both choices enable faster air path and hence torque response. First, a closed EGR valve reduces the long period of eliminating the residuals and replenishing with fresh air the manifold. Second, a closed wastegate position will allow the turbocharger to operate at higher speed, and therefore needing less time to spin to even higher speeds enabling fast increases in the air flow. The responsive cylinder air path during closed EGR/WG allows near instantaneous changes in fuel delivery and fast torque increases during tip-in. This strategy however comes with a fuel penalty due to high back pressures and elevated NOx emissions at low engine loads. The eSC decreases the torque response time, which enables WG and EGR valve to be opened at part loads and low engine speeds, which subsequently improves NOx emissions and fuel economy. The results of such a scenario are shown in Figure 14. As plotted, opening the EGR and WG valves more than their baseline values during low load operation (t<50 s) reduces BSFC by ≈4.6%. This, on the other hand, slows down the engine response to a torque increase request (notice $T_e$ for the base line engine with high EGR and open WG at low load). LP supercharging solves this torque increase deficiency and improves it to a rate even faster than the baseline engine with low EGR and closed WG.

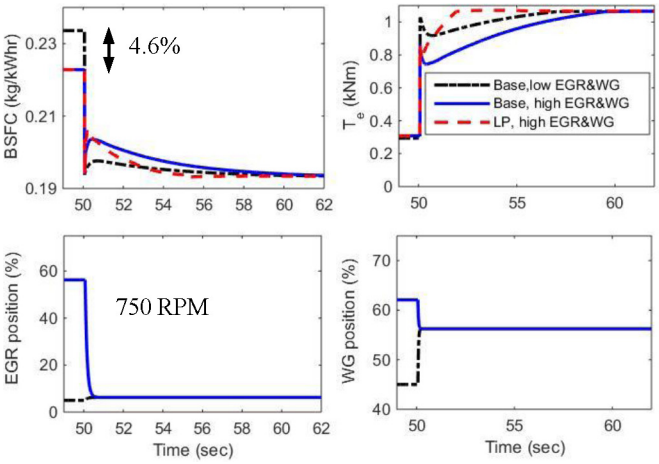


Figure 14. Using the eSC during a transient along with opening the WG and EGR valves at low load of steady states to improve both transient and steady state performance.

The advantage of opening the EGR and WG valves during steady state operation, and its corresponding fuel savings, is calculated from the fuel- energy ratio (FER) over the period of [T-Δt, T]:

$$FER = \frac{\int_{T-\Delta t}^{T} W_f . dt}{\int_{T-\Delta t}^{T} PW_{net} . dt} \quad (6)$$

with $PW_{net} = PW_{Eng} - PW_{EM}/\eta_{alt}$ and Δt indicating the integral window length. To compare with the FER of the baseline engine (which runs at low EGR and WG), the normalized FER $FER_{norm}=FER/FER_{base}$ is the defined and results for two different time windows are shown in Figure 15. As Figure 15-a shows, during the period of tip-in to settling time (from t = 50 to 62 s), both the baseline engine with low EGR and the supercharged engine with high EGR have the same fuel efficiency, however the supercharged engine has a faster torque response (Figure 14). When the integration window is extended so that 18 seconds is spent at low load with an open EGR valve, and then the tip-in happens, a fuel benefit of 1.5% along with a faster torque increase are possible with the supercharged engine (Figure 15-b).

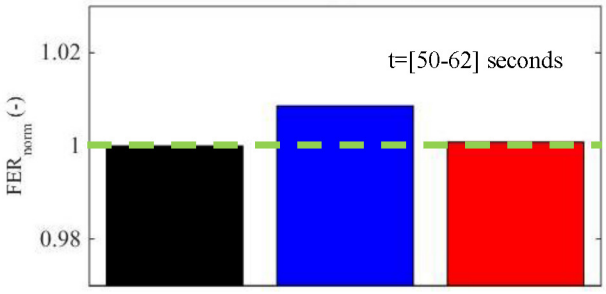


(a).

Figure 15.

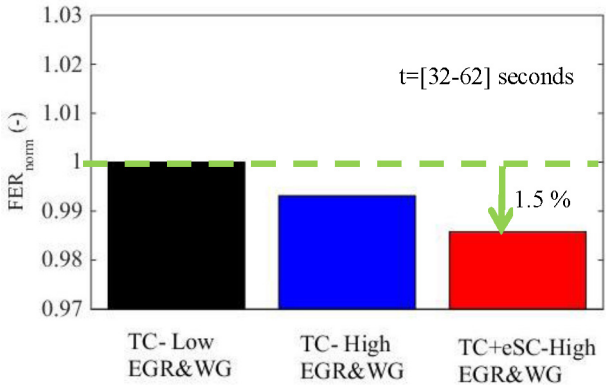


(b).

Figure 15 (cont.). The effect on fuel-energy ratio of opening the EGR and WG valves in conjunction with supercharging.

## Conclusions and Future Work

In this study, the effect of electric supercharger integration location on the performance of a turbocharged heavy duty diesel engine was studied for both steady state and transient operation. The study used a baseline turbocharged engine model which was compared to two possible configurations with an electrical supercharger, the first a low pressure (LP) implementation with the supercharger before the main compressor, and the second a high pressure (HP) implementation after the main compressor. Steady state supercharged engine operation showed that while the LP and HP configurations were able to increase low-end torque, the LP implementation was more efficient at low engine speeds. The HP configuration was more advantageous at part to high engine speeds. For the transient study, the FTP heavy duty transient drive cycle was analyzed to calculate the maximum cycle-based engine torque change. Step torque demands at constant engine speeds were also studied as ideal cases for evaluating engine transient response. During the FTP drive cycle, electric supercharging was required only at very low engine speeds to eliminate the fuel limited conditions associated with turbocharger response constraints. When the fast (step) torque demands were applied, a lack of air was observed during baseline engine load transients for all engine speeds. The electric supercharger was capable of improving air system transient response at low and medium engine speeds, but was much less effective beyond 1600 RPM. Since the engine efficiency generally improved with engine load, the supercharger's effect on load increase completely balanced the electric power consumption used for driving the supercharger. In addition, the simulations showed that at low to mid engine speeds (where the turbo lag is very evident) both the LP and HP integrations have similar performance. But due to higher corrected mass flows of the LP electric supercharger configuration, the supercharger isentropic efficiency dropped much more than the HP one as the engine speed increased. However, the difference between the LP and HP units observed during high engine speed transients was almost half of that observed at steady state operation. Simple control logic for the supercharger bypass valve provided insight on the hardware requirements. Specifically, the electric supercharger bypass valve should be twice as fast as the electric motor for effective supercharger performance. Finally, with the improved transient torque response of the supercharger, it was possible to open the WG and EGR valve at low engine speed and loads, which improved engine fuel economy by 4.6% at these low engine speeds and loads.

The work will be extended in future to study the effect of the eSC's compressor size on the HP and LP performance. In addition, by including a driver model and a more sophisticated control strategy for the eSC along with emission models, it would be possible to further investigate the effect of the eSC on fuel consumption and emissions during a full transient drive cycle.

## References


1. Ostrowski, G., Neely, G., Chadwell, C., Mehta, D. et al., "Downspeeding and Supercharging a Diesel Passenger Car for Increased Fuel Economy," SAE Technical Paper 2012-01-0704, 2012, doi:10.4271/2012-01-0704.
2. Banks A., Cornwell R. and Such C., "Advanced boosting technology to meet future heavy duty diesel engine requirements," In 11th International Conference on Turbochargers and Turbocharging, Oxford, pp. 241-250, 2014.
3. Linsel J. and Wanner S. "Two-stage Supercharging with a Scroll-type Supercharger and an Exhaust Gas Turbocharger", MTZ Worldwide, vol. 76 (11), pp.18-23, 2015.
4. Newman P., Luard N., Jarvis S., Richardson S., Smith T., Jackson R., Rochette C., Lee D. and Criddle M., "Electrical supercharging for future diesel powertrain applications," In: 11th Int. Conf. on Turbochargers and Turbocharging, London, pp. 207-216, 2014.
5. Benjey R.P.,Biller B. and Tsourapas V., "Cost effective hybrid boosting solution with application to light duty vocational vehicles," Int. J. Powertrains, vol. 4 (3), 2015, doi: 10.1504/IJPT.2015.071733.
6. Copeland C., Martinez-Botas R., Turner J., Pearson R., Luard N., Carey C., Richardson S., Di Martino P. and Chobola P., "Boost system selection for a heavily downsized spark ignition prototype engine, " In 10th International Conference on Turbochargers and Turbocharging, Oxford, pp. 27-41, 2012.
7. Morris G., Criddle M., Dowsett M., Heason T., Kapus P. and Neubauer M., "A New Engine Boosting Concept with Energy Recuperation for Micro/Mild Hybrid Applications," In 22nd International AVL Conference: Engine & Environment, 2010.
8. Birckett A., Tomazic D., Bowyer S., Bevan K., Wetzel P., Keidel S. and Biller B., "Transient Drive Cycle Modeling of Supercharged Powertrains for Medium and Heavy Duty On-Highway Diesel Applications, " SAE Technical Paper 2012-01-1962, 2012, doi:10.4271/2012-01-1962.
9. Keidel S., Wetzel P., Biller B., Bevan K. and Birckett A., "Diesel Engine Fuel Economy Improvement Enabled by Supercharging and Downspeeding," *SAE Int. J. Commer. Veh.* 5(2):2012, doi:10.4271/2012-01-1941.
10. Pohorelsky L., Brynych P., Macek J., Vallaude P.Y., Ricaud J.C., Obernesser P. and Tribotté P., "Air System Conception for a Downsized Two-Stroke Diesel Engine," SAE Technical Paper 2012-01-0831, 2012, doi:10.4271/2012-01-0831.
11. Salehi R., Stefanopoulou A.G., "Effective Component Tuning In A Diesel Engine Model Using Sensitivity Analysis," ASMEDSCC2015, Columbus, 2015.
12. Stefanopoulou A. and Smith R. "Maneuverability and smoke emission constraints in marine diesel propulsion," Control Engineering Practice, vol. 8(9), pp.1023 - 1031, 2000.
13. Code of federal regulation (CFR), "Control of emissions from new and in-use highway vehicles and engines", Title 40, Chapter I, Subchapter C, Part 86, 2015


## Contact Information


Rasoul Salehi
University of Michigan, Ann Arbor
rsalehi@umich.edu


## Acknowledgment


The authors would like to thank Detroit Diesel Corporation (DDC) for providing part of the DD13 engine data used in this work.


## Definitions/Abbreviations

**AFR** - Air fuel ratio

**BSFC** - Brake specific fuel consumption

**DPF** - Diesel particular filter

**EGR** - Exhaust gas recirculation

**EM** - Electric motor

**eSC** - Electric supercharger

**FER** - Fuel energy ratio

**FTP** - Federal Test Procedure

**HDD** - Heavy Duty Diesel

**HD** - Heavy duty

**HP** - High Pressure

**LP** - Low Pressure

**WG** - Wastegate


The Engineering Meetings Board has approved this paper for publication. It has successfully completed SAE's peer review process under the supervision of the session organizer. The process requires a minimum of three (3) reviews by industry experts.





ISSN 0148-7191

http://papers.sae.org/2016-01-1035